# Depth-Sensitive Cerebral Blood Flow and Low-Frequency Oscillations for Consciousness Assessment Using Time-Domain Diffuse Correlation Spectroscopy

Sahar Sabaghian[1], Chien-Sing Poon[2], Carsi Kim[1], Christopher H Moore[1], Irfaan Dar[1], Timothy M. Rambo[3], Aaron J. Miller[3], Sujith Swarna[4], Noah Lubin[4], Sima Mofakkam[4], Charles Mikell[4], Jingxing Wang[4], Brandon Foreman[5], and Ulas Sunar[1*]

*[1]Dept of Biomedical Engineering, Stony Brook University, Stony Brook, NY, USA*
*[2]Dept of Biomedical Engineering, Wright State University, Dayton, OH, USA*
*[3]Quantum Opus LLC*
*[4]Dept of Neurosurgery, Stony Brook University, Stony Brook, NY, USA*
*[5]Dept of Neurology & Rehabilitation Medicine, University of Cincinnati, Cincinnati, OH, USA*
**ulas.sunar@stonybrook.edu*

**Abstract:** This study evaluates the feasibility of depth-sensitive bedside monitoring of cerebral blood flow (CBF) and low-frequency oscillations (LFOs) using time-domain diffuse correlation spectroscopy (TD-DCS) in healthy controls, comatose patients, and subjects in the Minimally Conscious State (MCS). A 1064 nm TD-DCS system equipped with superconducting nanowire single-photon detectors (SNSPDs) was used to collect 10-minute resting-state data from 25 healthy adults, 3 comatose patients with traumatic brain injury (TBI), and 2 patients with MCS in the subacute phase. Photon arrival times were temporally gated to distinguish superficial and cortical tissue contributions. The blood-flow index (BFI) was extracted from gated autocorrelation functions, and LFOs were quantified using power spectral density within the Slow-5 (0.01-0.027 Hz), Slow-4 (0.027-0.073 Hz), and Slow-3 (0.073-0.198 Hz) bands. Resting-state LFO power progressively decreased from healthy individuals to MCS and comatose patients, consistent with impaired neurovascular coupling and diminished autoregulatory function in severe consciousness impairment. An auditory "smile" command was delivered to five healthy subjects, one MCS patient, and one Unresponsive Wakefulness Syndrome (UWS) patient to assess task-evoked hemodynamic responses. During the smile task, healthy participants showed clear hemodynamic responses, whereas the MCS and UWS patients demonstrated smaller and more rapidly decaying responses. Overall, TD-DCS provides a noninvasive, depth-resolved approach for differentiating consciousness states and identifying residual cortical responsiveness, supporting its potential for bedside neurocritical-care monitoring.

**Keywords:** cerebral blood flow; disorders of consciousness; low-frequency oscillations; time-domain diffuse correlation spectroscopy; traumatic brain injury.

## Introduction

Acute brain injury (ABI) is a leading cause of mortality and long-term disability, particularly among young adults [1–4] . While the primary injury occurs at the moment of trauma, secondary processes such as impaired autoregulation, ischemia, and inflammation can evolve over hours to days, driving further neurological deterioration [5,6]. Continuous bedside monitoring of cerebral blood flow (CBF) is therefore critical for detecting secondary injury and guiding timely intervention [7–13].

Conventional imaging techniques such as magnetic resonance imaging (MRI), computed tomography (CT), and positron emission tomography (PET) provide detailed structural and functional information but are limited by their high cost, logistical complexity, and lack of feasibility for continuous bedside monitoring [14]. Diffuse correlation spectroscopy (DCS) offers a non-invasive and portable alternative capable of tracking microvascular CBF in real time. Compared to near-infrared spectroscopy (NIRS), DCS provides greater sensitivity to cerebral blood flow and has shown promise in neurocritical care applications [11,15,16]. However, standard continuous-wave (CW) DCS systems are limited in depth specificity and can be influenced by signals from superficial tissues such as the scalp and skull [17–19].

Time-domain DCS (TD-DCS), enhances depth sensitivity by isolating late-arriving photons that have traveled deeper into tissue [20–22]. When implemented at longer wavelengths such as 1064 nm and combined with highly sensitive detectors such as SNSPDs, TD-DCS enables deeper penetration, improved signal-to-noise ratio, and higher permissible laser power, making it well-suited for adult human brain monitoring [23–33]. While cerebral blood flow parameter provides one indication of brain health, spontaneous low-frequency oscillations (LFOs) in the range of 0.01-0.2 Hz are known to reflect important physiological processes including endothelial, neurogenic, and respiratory activity, and have been associated with cerebrovascular regulation and brain function [31,34–53]. Optical bedside monitoring of cerebral hemodynamics in brain injury has been demonstrated using DCS (e.g.,[54–65]). However, few studies have focused on low-frequency oscillations (LFOs), and their depth-specific characterization in acute human brain injury remains largely unexplored.

Disorders of Consciousness (DOCs) represent a clinical spectrum of severe cerebral dysfunction, ranging from coma, a state of unarousable unresponsiveness where the eyes remain closed and no signs of awareness are present, to chronic states of impaired consciousness. These chronic states include the Unresponsive Wakefulness Syndrome (UWS) (formerly known as the Vegetative State), characterized by preserved arousal with no evidence of purposeful behavior or awareness, and the Minimally Conscious State (MCS), defined by inconsistent but reproducible signs of awareness, such as visual tracking, localization, or command following [66, 67] .

Accurate differentiation between UWS and MCS remains difficult, with misdiagnosis rates of 30–40% when relying solely on clinical examination [45,68–70]. Neuroimaging and neurophysiological modalities, including fMRI [71–73], PET [74–77], EEG [75,78,79–82], and NIRS [83–86] , have enabled detection of MCS/covert consciousness, in which patients demonstrate preserved cortical activation despite absent behavioral output. However, these techniques are limited by either lack of portability (fMRI, PET) or depth specificity (EEG, NIRS), constraining their feasibility for repeated bedside assessments in critically ill patients. Electroencephalography (EEG) provides bedside compatibility and high temporal resolution but suffers from low spatial specificity, susceptibility to

artifacts, and reduced sensitivity to deep cortical responses, particularly in patients with skull defects [81,87,88]. Functional NIRS has recently shown promise in detecting task-evoked responses using personalized motor-speech imagery and covariance-based classifiers [89–91], yet it remains limited by superficial contamination and reliance on surrogate oxygenation measures.

While resting-state signals and oscillations can provide insight into baseline physiology, task-evoked functional responses may offer greater contrast for assessing consciousness states by detecting residual cortical reactivity. Auditory or command-driven paradigms such as familiar voices or simple motor tasks elicit reproducible hemodynamic responses in conscious patients but are absent in deeply unconscious states[45,92–94] . These paradigms are commonly studied with functional MRI (fMRI), which is impractical in intensive care unit (ICU) settings. In this study, we incorporated auditory stimulation tasks, which elicit reproducible hemodynamic responses in patients with residual consciousness [45–53,92].

Time-domain diffuse correlation spectroscopy (TD-DCS) addresses these limitations by directly measuring cerebral blood flow (CBF) and its spontaneous fluctuations in a depth-sensitive, non-invasive manner. Unlike NIRS- or BOLD-based techniques that rely on surrogate markers of oxygenation, TD-DCS quantifies microvascular flow dynamics with high temporal resolution and deep-tissue sensitivity when implemented at 1064 nm with superconducting nanowire single-photon detectors. This configuration enables deeper tissue penetration, improved signal-to-noise ratio, and higher laser safety limits, making it a realistic alternative to fMRI in longitudinal consciousness assessment and neurocritical-care monitoring [10,95–101] .

By combining the portability and bedside practicality of fNIRS and EEG with the physiological specificity of perfusion imaging, TD-DCS offers a unique opportunity for repeated, real-time assessment of brain function in DOC patients without requiring transport or complex infrastructure. In this study we evaluate the utility of TD-DCS in both resting-state and task-evoked paradigms to detect residual cortical reactivity and differentiate levels of consciousness in critically ill patients as a potential bedside adjunct for neurocritical-care monitoring.

## Materials and Methods

### Study Design and Patient Details

This study is a retrospective analysis of a prospective, observational protocol designed to evaluate CBF in healthy individuals and patients with traumatic brain injury (TBI). A total of 25 healthy adult volunteers (14 male, 11 female) were recruited at Wright State University in 2022. Additionally, five patients with TBI were enrolled between 2022 and 2025 from the University of Cincinnati Medical Center and Stony Brook University Hospital, respectively. All healthy participants provided written informed consent under a protocol approved by the Institutional Review Boards (IRBs) of Wright State University and Stony Brook University. The study was conducted in accordance with the Declaration of Helsinki and approved by the IRBs of Wright State University, Stony Brook University, and the University of Cincinnati Medical Center. For TBI patients, informed consent was obtained from legally authorized representatives in accordance with these IRB approvals. For analysis, we extracted 10 minutes of resting-state baseline data from each subject. In TBI patients, recordings were performed in the intensive care unit (ICU) during routine monitoring, with patients remaining at rest and receiving standard clinical care. No

experimental interventions were introduced, and no restrictions were placed on medical treatment during the data acquisition period.

## TD-DCS System for Data Acquisition

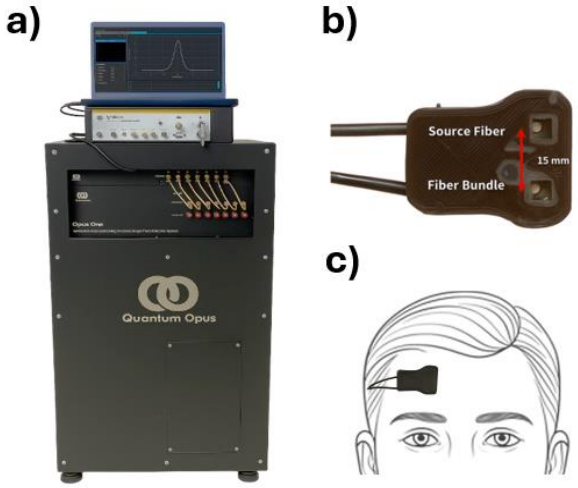


**Figure 1. Overview of the time-domain diffuse correlation spectroscopy (TD-DCS) system**. a) Quantum Opus superconducting nanowire single-photon detector (SNSPD) system with the VisIR pulsed laser (1064 nm) mounted on top. The display shows the photon distribution of time-of-flight (DTOF). b) Close-up view of the custom 3D-printed probe with a 15 mm source-detector separation between the source and detector fibers. c) Example of the probe placed on the right forehead of a human subject for cerebral blood flow measurements.

The TD-DCS method has been employed in numerous previous studies, demonstrating its feasibility for clinical use [102–111] . Figure 1a-c illustrates the components of the system and probe placement**.** The optical imaging probe was positioned on the right forehead, between EEG scalp locations F4 and F8, to ensure consistent and anatomically relevant placement. The probe incorporated a 600-µm-core multimode source fiber (NA = 0.39, FT600EMT, Thorlabs, NJ, USA) and an 8.2-µm-core detector fiber (SMF-28, Thorlabs, NJ, USA), which is few-mode at 1064 nm[112]. The source-detector separation (SD) was fixed at 15 mm, a spacing selected to optimize sensitivity to cerebral tissue while maintaining a high signal-to-noise ratio (SNR) in adults, based on prior modeling and experimental studies. All fibers were aligned through a 5 mm right-angled prism and embedded in a custom-designed, flexible 3D-printed housing optimized for ergonomic use in clinical environments. The probe's contact footprint was approximately 25 mm × 25 mm, slightly larger than a US quarter, minimizing scalp contact while enabling secure and reproducible placement. The assembly was affixed using medical-grade Tegaderm film (3M, Saint Paul, MN) following sterilization with alcohol swabs. Reflected photons at 1064 nm were detected using four superconducting nanowire single-photon detectors (SNSPDs), which were interfaced with a 4-channel time-correlated single-photon counting (TCSPC) system (HydraHarp400, PicoQuant GmbH, Berlin, Germany) [113,114].

Two excitation sources were employed depending on the subject group. For the Healthy participants (n = 25) and the comatose TBI patient measured at the University of Cincinnati Medical Center, a 1064 nm pulsed seed laser (QC2D106P-64D0, QDLaser Inc., Kanagawa, Japan) operating at an 80 MHz repetition rate with a 250 ps pulse width was used. For the MCS patients and the comatose patients recorded at Stony Brook University Hospital, as well as for functional task measurements (Smile Protocol), a 1064 nm pulsed laser (VisIR-1064-HC High-

Coherence, PicoQuant GmbH, Berlin, Germany) operating at an 80 MHz repetition rate with a 400 ps pulse width was used. The beam exiting the prism face was expanded to approximately 4.5 mm in diameter using a diffuser film to ensure uniform illumination across a large beam area. The average power was kept below ANSI safety limits, and each detection channel operated at a photon count rate of ~1 × $10^7$ counts per second (cps).

## Data analysis

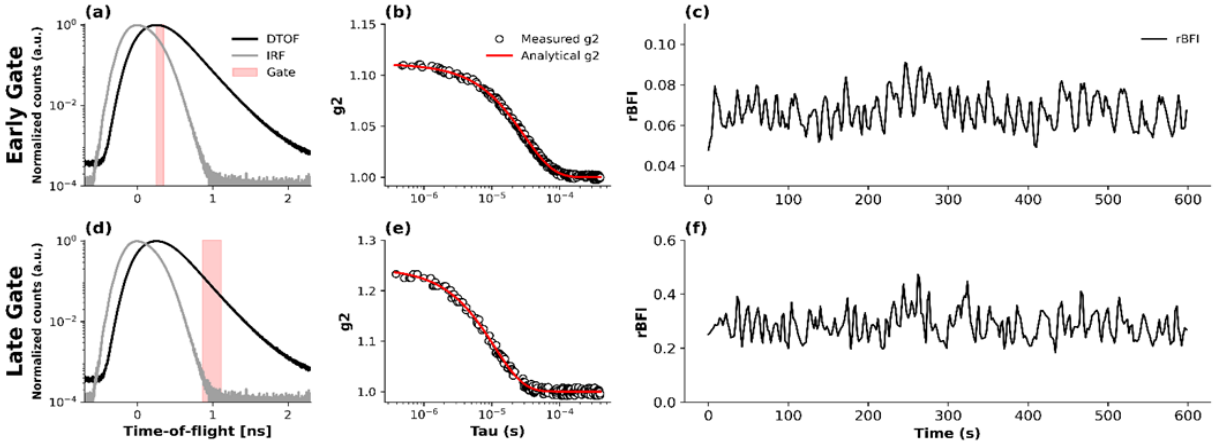


**Figure 2**. **Early- and late-gate analysis of TD-DCS measurements**. (a,d) Normalized distributions of time-of-flight (DTOF, black) and instrument response function (IRF, gray), with the selected gate window shown in red for the early and late gates, respectively. (b,e) Corresponding normalized intensity autocorrelation curves $g_2(\tau)$ (black circles) and analytical fits (red lines) used to estimate the blood-flow index (BFI). (c,f) Temporal evolution of the relative blood-flow index (rBFI) derived from the early and late gates, respectively, showing increased fluctuation amplitude and deeper sensitivity for the late-gate signal.

Time-tagged photon arrival data were recorded continuously and segmented into 10-minute intervals, yielding approximately 140 GB of data. Data processing was performed using a custom MATLAB routine on a high-memory computing node with 1.5 TB of RAM. The instrument response function (IRF) was characterized by placing a thin scattering layer (Teflon tape, 3M) between the source and detector fibers during a 30-second calibration, resulting in a full width at half maximum (FWHM) of ~400 ps for the VisIR-1064-HC [115] . Two temporal gates were selected based on the distribution of time-of-flight (DTOF). The early gate (EG), centered at 0.20 ns with a width of 100 ps, was positioned just after the DTOF peak to emphasize photons that predominantly sampled superficial tissue layers (Fig. 2a). The late gate (LG), centered at 1.03 ns with a width of 250 ps, was placed on the decaying slope of the DTOF to enhance sensitivity to deeper tissue regions (Fig. 2d). Gate positions were defined relative to the peak of the combined DTOF across all channels to maintain consistent depth sensitivity among subjects. This strategy was designed to capture photons from deeper tissue layers while minimizing contamination from superficial dynamics. It aligns with prior findings that optimally selected narrow time gating (e.g., 100 ps) with sufficient SNR can enhance depth specificity in TD-DCS [116]. As motivated by

Tagliabue et al.[117], who demonstrated spatial and temporal optical heterogeneity in injured brains, we performed subject-specific fitting of the temporal point spread function (TPSF) to extract optical parameters ($\mu_a$, $\mu_s'$) as *a priori* inputs for the analytical intensity autocorrelation functions ($g_2$) fitting to quantify blood flow index (BFI). The $g_2$ functions were extracted directly from each gate using delay times ranging from $5 \times 10^{-7}$ to $1 \times 10^{-3}$s. Autocorrelations were calculated using 5 s integration windows with 1 s step size, producing overlapping data segments to enhance temporal resolution (Figs. 2b, e). The resulting $g_2$ curves were fitted to an analytical model derived from the time-domain diffusion equation. Because detection was performed with an 8.2 μm-core few-mode fiber, the measured β values were relatively low compared with those typically obtained in single-mode DCS systems (β~0.5), resulting in smaller $g_2$ amplitudes (Figs. 2b, e). Although this configuration reduces temporal coherence, it substantially improves the signal-to-noise ratio (SNR), which is critical for reliable estimation of cerebral blood flow in human measurements. The final relative blood-flow index (rBFI) values were obtained by fitting averaged $g_2$ curves from all four detection channels (Figs. 2c, f).

**Power Spectral Density Analysis for Low-Frequency Oscillations (LFOs)**

In addition to evaluating cerebral blood flow changes, we analyzed LFOs in the blood flow index as potential indicators of cerebrovascular function. LFOs were defined as spontaneous fluctuations occurring below 0.5 Hz and examined within three frequency ranges (summarized in Table 1) that have been linked to specific physiological mechanisms: Slow-5 (0.01-0.027 Hz, endothelial/cerebral autoregulation), Slow-4 (0.027-0.073 Hz, neurogenic activity/brain function), and Slow-3 (0.073-0.198 Hz, respiratory or brain-stem-driven fluctuations) [34,48,118,119]. Frequency ranges dominated by Mayer waves and higher-frequency systemic noise (Bands I and II) were excluded from further analysis. For each subject and condition, the rBFI time series was detrended using a second-order polynomial and then band-pass filtered (0.01-0.4 Hz) with a zero-phase Butterworth filter to isolate low-frequency components. Power spectral density (PSD) was then computed using the fast Fourier transform (FFT). Total low-frequency power, $P_{\text{total}}$, was computed by integrating the PSD over 0.01-0.4 Hz using the trapezoidal rule, which reflects the overall amplitude of low-frequency rBFI fluctuations.

**Table-1:** Frequency bands for low-frequency oscillations (LFOs) with respect to band-1 to band-5, and

| Band | Frequency Range (Hz) | Possible Mechanism |
|---|---|---|
| V | 0.01-0.027 | Endothelial (cerebral autoregulation, CA) |
| IV | 0.027-0.073 | Neurogenic (neural activation/brain function) |
| III | 0.073-0.198 | Respiratory or brain function (lower frequencies) |
| II | 0.198-0.5 | Mayer waves (arterial blood pressure, ABP) / Respiratory |
| I | 0.5-0.75 | Mayer waves (arterial blood pressure, ABP) |

To compare spectral shape across subjects, each PSD was normalized by its own total low-frequency power and interpolated onto a common frequency axis between 0.01 and 0.4 Hz (see Figs. 3c, g for representative group-averaged normalized PSDs). For band-limited metrics, band power in each LFO range, $P_B$, was obtained by integrating the unnormalized PSD over the corresponding frequency interval. Normalized band power was defined as the fraction of low-frequency power in each band, $R_B = P_B/P_{\text{total}}$, such that $R_B$ represents the proportion of total 0.01-0.5 Hz rBFI power allocated to Slow-5, Slow-4, or Slow-3. Mean and standard error of $P_{\text{total}}$ and $R_B$ were then calculated for each group and gate. We note that arterial blood pressure (ABP) was not recorded in this feasibility study. Unlike transfer-function analyses of autoregulation that require ABP as an input signal (e.g., [120–125] ), our approach focuses on the output fluctuations of the TD-DCS blood-flow index and on the relative distribution of power across physiologically motivated frequency bands.

## Results

### Resting-State and Auditory Task in Healthy and TBI Subjects

### Healthy Subjects

TD-DCS measurements were performed in two distinct cohorts of healthy adult participants. 1. Resting-State Measurements: A subset of 25 healthy adults was recruited to assess baseline cerebral hemodynamics. TD-DCS data were collected over a 10-minute resting period, during which participants lay in a supine position on a hospital bed with no task engagement or external stimuli. 2. Auditory Task Evaluation: To evaluate functional cerebral responses, an auditory stimulation task was performed in a separate cohort of five healthy subjects. This protocol involved delivering the verbal command of “smile” approximately every 60 seconds, for a total of five repetitions. This protocol was used to evaluate task-evoked functional responses [71,83,126] and provided a comparison for subsequent patient data. TD-DCS allowed continuous data acquisition throughout the session and then applied in two TBI cases as detailed below.

### Case Study 1: Traumatic Brain Injury Patient - Minimally Conscious State (MCS)

Two individuals TBI were included and clinically assessed as being in the Minimally Conscious State. Both were evaluated at academic medical centers during the subacute phase of recovery. The first patient was an adult male in his 40s who sustained a traumatic brain injury and subsequently met clinical criteria for MCS. TD-DCS measurements were performed at the bedside in the intensive care setting and included a 10-minute resting-state recording followed by an auditory command task. During the task, the verbal cue “smile” was delivered approximately every 60 seconds for a total of five repetitions, with continuous TD-DCS acquisition throughout. The second patient was an adult male in his 70s, also diagnosed with MCS based on clinical evaluation. A 10-minute resting-state TD-DCS measurement was performed in the intensive care setting to assess baseline cerebral blood-flow dynamics. No external stimulation was administered, and routine clinical care continued uninterrupted during the recording period.

.

## Case Study 2: Traumatic Brain Injury Patient – Unresponsive Wakefulness Syndrome (UWS)

One individual with traumatic brain injury was clinically assessed as being in the Unresponsive Wakefulness Syndrome. The patient was an adult male in his 40s who presented with severe neurological impairment in the subacute phase of recovery. TD-DCS measurements were performed at the bedside in the intensive care setting using an auditory command paradigm to evaluate potential functional reactivity. During this task, the verbal cue “smile” was delivered approximately every 60 seconds for a total of five repetitions, with continuous bilateral TD-DCS acquisition. A dual-probe configuration was used to record simultaneous measurements from both hemispheres, enabling within-subject comparison of hemodynamic responses. One hemisphere served as a control region, while the contralateral side had a history of prior neurosurgical intervention. This setup allowed assessment of potential asymmetries in cortical reactivity associated with the patient’s injury. The bilateral TD-DCS measurements provided complementary depth-sensitive information on functional vascular dynamics across hemispheres during the auditory stimulation paradigm.

## Case Study 3: Traumatic Brain Injury Patients - Coma State

Three individuals with traumatic brain injury were clinically assessed as being in a comatose state and underwent TD-DCS monitoring at two academic medical centers. For all three patients, a 10-minute resting-state TD-DCS measurement was performed at the bedside in the intensive care setting to evaluate baseline cerebral perfusion. No external stimulation was administered, and routine clinical care continued during all recordings. The first patient was an adult male in his late 20s who remained unresponsive throughout the recording session. The second patient was an adult male in his 40s, who also remained comatose during monitoring. The third patient was an adult male in his 70s with significant neurological impairment, similarly, demonstrating no behavioral responsiveness during the TD-DCS session. These recordings provided depth-sensitive physiological data across a range of severe TBI presentations within the comatose state.

## Depth-Sensitive Blood Flow and LFO in Resting State

The Mean BFI, a measurement used as a proxy for CBF, was assessed using TD-DCS in three subject groups: Healthy controls (n=25), Coma patients (n=3), and Minimally Conscious State (MCS) patients (n=2). The TD-DCS method allowed for the distinction between blood flow in the superficial tissue, presented in the Early Gate (Figure 3a), and the deeper, cerebral tissue, presented in the Late Gate (Figure 3e). Analysis of the superficial BFI (Early Gate, Figure 3a) revealed a progressive increase across the groups. Healthy controls registered the lowest mean BFI, approximately 0.28× $10^{-7}\ mm^2/s$. The BFI was substantially elevated in the Coma group, averaging around 1.02 × $10^{-7}\ mm^2/s$, though this group displayed notable inter-subject variability as indicated by the error bar. The highest superficial BFI was observed in the MCS group, approximately 1.60 × $10^{-7}\ mm^2/s$. A consistent pattern of elevated flow was observed in the Cerebral BFI (Late Gate, Figure 3e). Here, Healthy controls measured approximately 1.26 × $10^{-7}$ $mm^2/s$. Similar to the superficial layer, the BFI increased in the DOC groups, rising to approximately 2.57 × $10^{-7}\ mm^2/s$ for the Coma group and peaking at approximately 3.54 × $10^{-7}$

$mm^2/s$ for the MCS group. The results indicate that the BFI is significantly elevated across both the superficial and deep tissue compartments in patients with Disorders of Consciousness, with the Minimally Conscious State group consistently exhibiting the highest blood flow index. This consistent finding suggests a potential systemic neurovascular dysregulation or ongoing inflammatory process following severe brain injury.

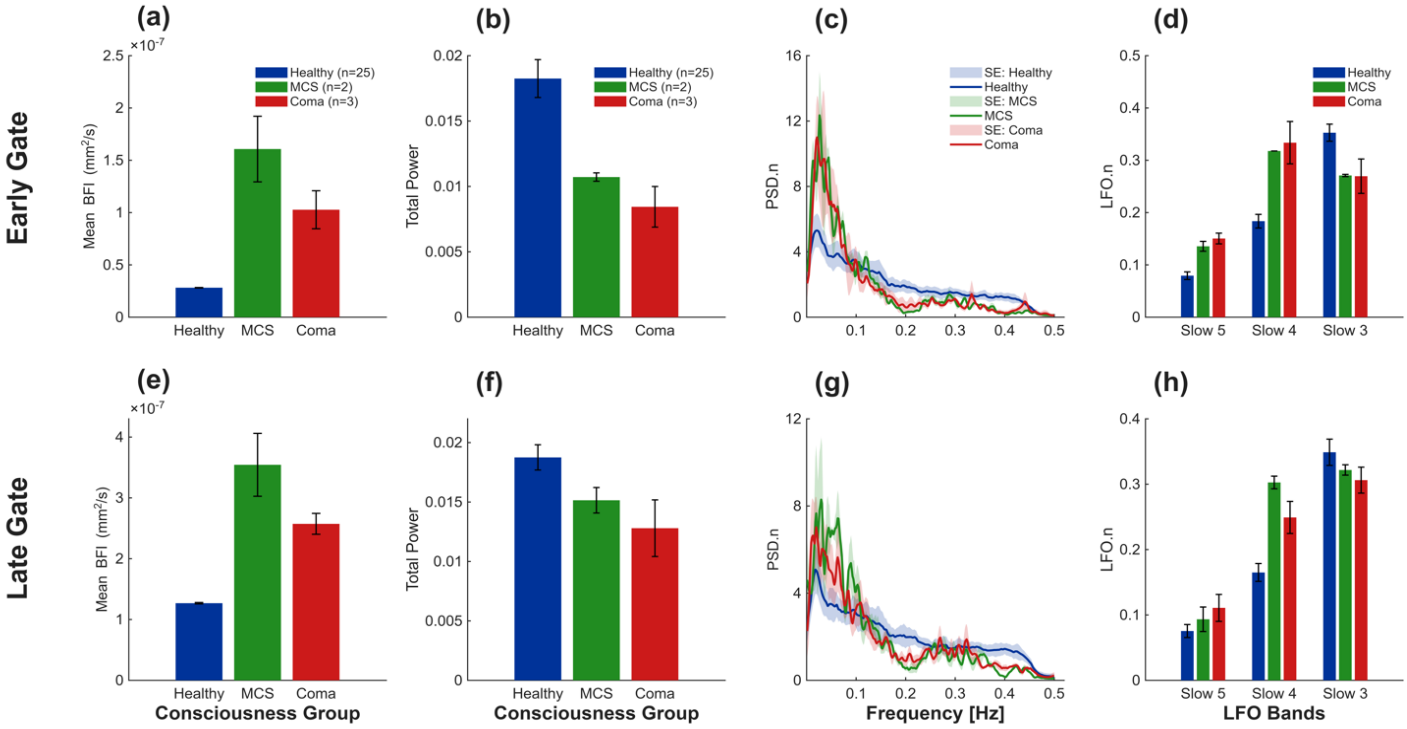


**Figure 3. Early-gate and late-gate depth-resolved analysis of resting-state blood-flow fluctuations across consciousness groups**. Panels (a–d) summarize Early Gate (EG) results, while panels (e–h) show corresponding Late Gate (LG) findings. (a,e) Mean BFI (mm²/s) averaged across subjects in each group (Healthy: n=25; MCS: n=2; Coma: n=3), with error bars representing SEM. (b,f) Total Power of low-frequency oscillations (0.01–0.40 Hz) computed using trapz-integrated PSD, showing overall LFO amplitude differences across groups. (c,g) Group-averaged normalized PSD (PSD.n) with shaded standard error, demonstrating the spectral distribution of resting-state fluctuations across the 0.01–0.50 Hz band. (d,h) Band-specific normalized LFO power (LFO.n) for Slow-5 (0.01–0.027 Hz), Slow-4 (0.027–0.073 Hz), and Slow-3 (0.073–0.198 Hz), illustrating depth-dependent differences in oscillatory power across consciousness states. Healthy controls exhibit stronger contributions from higher-frequency Slow-3 content, while DOC patients display dominant Slow-4 activity in both EG and LG, consistent with impaired neurogenic regulation. These findings indicate that despite preserved deep oscillatory power, DOC patients exhibit frequency-specific disruption of vascular control systems, most notably in neurogenic bands.

The depth-resolved analysis of resting-state low-frequency oscillations (LFOs) revealed clear distinctions in vascular fluctuation amplitude and spectral organization across consciousness groups. In the superficial early-gate (EG) measurements (Fig. 3b), Healthy individuals exhibited the highest Total Power (mean ≈ 0.018), whereas both minimally conscious state (MCS) and

Coma patients showed markedly reduced amplitudes (means ≈ 0.01 and ≈ 0.008, respectively). This attenuation of spontaneous LFO activity in the superficial layers suggests diminished vascular variability associated with impaired consciousness. In contrast, within the deeper late-gate (LG) measurements (Fig. 3f), Total Power values for MCS (mean ≈ 0.015) and Coma patients (mean ≈ 0.012) were more closely aligned with the Healthy group (mean ≈ 0.018). The reduced contrast between groups at depth indicates that deeper cortical regions retain more robust oscillatory dynamics even in severe brain injury, underscoring the increased cortical contribution captured by LG measurements and highlighting the importance of depth gating for probing preserved neurovascular function. The normalized Power Spectral Density (PSD.n) (Fig. 3c, g) further demonstrated systematic spectral reorganization across consciousness groups and depths. Healthy subjects displayed a broad distribution of LFO power across the 0.01-0.5 Hz range, whereas both MCS and Coma patients showed a clear shift toward very low-frequency content (< 0.1 Hz). This redistribution was evident in both EG and LG measurements but was most pronounced in the LG, where MCS patients exhibited the strongest concentration of normalized power at the lowest frequencies. Such enhancement of slow oscillatory components likely reflects impaired autoregulation, reduced neurogenic activity, and altered autonomic or endothelial signaling associated with severe brain injury. These spectral differences were quantified through normalized LFO band power (LFO.n) (Fig. 3d, h) across three canonical frequency bands, Slow-5 (0.01-0.027 Hz, endothelial), Slow-4 (0.027-0.073 Hz, neurogenic), and Slow-3 (0.073-0.198 Hz, respiratory). Healthy participants showed relatively stronger contributions from the higher-frequency Slow-3 band, consistent with preserved physiological variability and intact neurovascular control. In contrast, both DOC groups demonstrated a marked elevation in Slow-4 power, which emerged as the dominant LFO component in both EG and LG data. This shift toward Slow-4 dominance, especially in deeper cortical signals, suggests impaired neurovascular coupling and dysregulated autonomic modulation following acute or chronic brain injury. Overall, the depth-resolved resting-state analysis indicates that LFO alterations in disorders of consciousness manifest as both reduced amplitude and redistribution of spectral power toward slower frequencies. These effects are more prominent in deeper cortical layers, supporting the use of late-gated measurements for capturing residual neurovascular dynamics. Together, these findings highlight the value of depth-sensitive LFO metrics as potential physiological markers of cerebrovascular integrity and neural function in patients with impaired consciousness.

**Depth-Sensitive Hemodynamic Responses to Auditory Stimulation**

While resting-state oscillations provide information on baseline physiology, task-evoked functional responses offer a critical method for assessing consciousness levels by providing greater contrast in brain activity. The simple auditory "smile" command was therefore employed to evaluate residual cortical responsiveness across subject groups, serving as a noninvasive bedside paradigm commonly used in neuroimaging studies of consciousness. This protocol involved administering the verbal instruction approximately every 60 seconds for a total of five repetitions, with the instruction phase lasting for 5 seconds. The utility of TD-DCS lies in its ability to separate the hemodynamic signals into layers, enabling depth-sensitive analysis of the evoked relative blood-flow index.

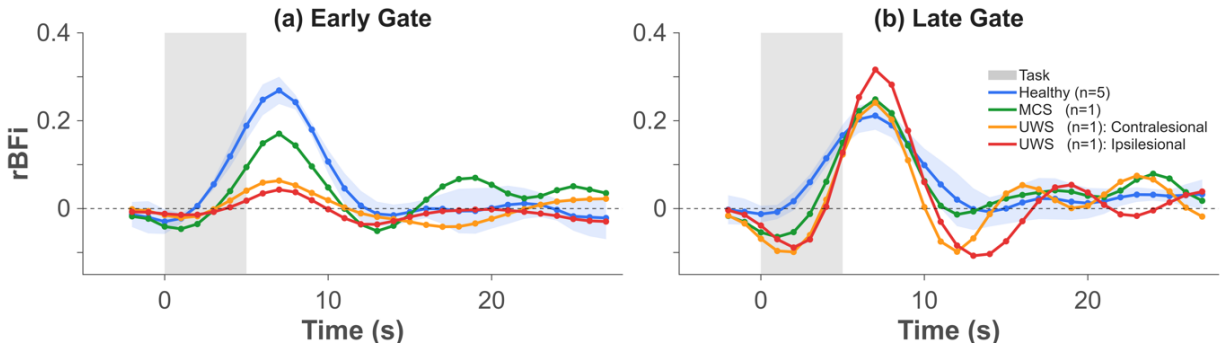


**Figure 4. Normalized blood-flow index responses during the Auditory "Smile" Task.** (a) The Early Gate signal, reflecting superficial tissue dynamics, shows a strong, rapid peak in Healthy subjects (n=5), which is attenuated in the MCS (n=1) and nearly flat in the UWS patient (n=1), indicating profound lack of superficial motor activity. (b) The Late Gate signal, reflecting deeper cerebral tissue, shows a canonical hemodynamic trajectory in Healthy controls. The MCS patient displays smaller but temporally aligned responses, suggesting partially preserved cortical reactivity. In the UWS patient, the ipsilesional (TBI) side shows a transient LG response with a modest peak around ~7 seconds and a rapid return to baseline. This response lacks the typical post-stimulus persistence and suggests non-sustained vascular dynamics rather than true cortical activation. The contralesional LG signal in the UWS patient remained low in amplitude and did not exhibit a distinct stimulus-locked peak, consistent with reduced cortical engagement on the non-injured hemisphere.

The Early Gate signal captures photons that primarily sample light travel through the superficial tissue layers, such as the scalp and skull, making it sensitive to non-cerebral vascular dynamics like facial muscle activity. As seen in Figure 4.a, in Healthy subjects, the EG signal displayed a strong and rapid peak immediately following the verbal cue. This robust and quick rise is consistent with superficial vasodilation related to the facial motion or preparation for the motor task. Conversely, the MCS patient exhibited a response that was noticeably attenuated compared to the healthy cohort. This diminished superficial signal reflects their severely limited or absent overt behavioral (motor) output, as some of the commands were physically followed. Similarly, the UWS patient showed minimal modulation or near to flat response in the early gate. The Late Gate signal isolates photons that have traveled deeper, significantly enhancing sensitivity to the deeper cerebral tissue and providing a direct assessment of cortical engagement and neurovascular coupling. As shown in Figure 4.b, Healthy subjects demonstrated the expected canonical hemodynamic trajectory in the LG signal: a gradual rise, a peak several seconds after stimulus onset, and a slow return to baseline, reflecting robust cortical activation. The MCS patient showed smaller but temporally aligned responses in the LG. This suggests the presence of partially preserved cortical reactivity despite the lack of motor output, serving as a key indicator of residual consciousness[71,72,127,128]. In the UWS patient, the ipsilesional (TBI) side (red dashed-dotted line) exhibited a transient LG response with a modest peak around ~7 seconds, followed by a rapid return to baseline. This trajectory lacked the sustained elevation typically observed in canonical cortical responses. Rather than reflecting preserved cortical engagement, this pattern suggests non-sustained or dysregulated vascular dynamics. The contralesional (control)

hemisphere (orange dotted line) showed a low-amplitude LG signal without a clear post-stimulus peak, consistent with reduced cortical engagement on the non-injured side. Together, this bilateral LG pattern in the UWS patient supports a profile of impaired neurovascular coupling and diminished cortical reactivity, characteristic of deep unconsciousness [73,129,130] .

## Discussion

This study demonstrates a novel application of TD-DCS for depth-sensitive assessment of CBF and spontaneous LFOs in healthy individuals and patients with TBI. Using a portable 1064 nm TD-DCS system with SNSPDs, we obtained depth-specific hemodynamic signatures associated with varying levels of consciousness and injury severity [26,27,131]. Our results highlight the ability of TD-DCS to distinguish superficial and cortical vascular dynamics. The total LFO amplitude in resting state decreased from Healthy to MCS to Coma reflecting altered neurovascular dynamics. This trend was most prominent in the cortical (late-gated) signal and aligns with prior reports from fNIRS and fMRI studies indicating that LFOs diminish with increasing severity of consciousness impairment. In particular, fNIRS studies such as Schulthess et al. [126] and Kazazian et al. [83] have demonstrated reduced spontaneous or task-evoked LFO activity in patients with unresponsive wakefulness syndrome (UWS), supporting the idea that LFO preservation reflects residual neurovascular reactivity and cortical engagement. These findings contrast with acute-phase animal studies (e.g., White et al., [132]) that reported increased LFOs shortly after injury, likely reflecting metabolic instability or pathological vasomotion in the hyperacute window. In the subacute clinical setting of our study, preserved LFOs are more likely to represent stable autoregulation and cortical viability. Given that our patients were studied in the subacute phase post-injury, the reduction in cerebral LFO power likely reflects impaired autoregulation and cortical silence rather than acute hyperactivity or inflammation. This aligns with the hypothesis that spontaneous LFOs serve as a surrogate for intact neurovascular coupling, and their suppression may indicate poor prognosis or severely disrupted brain function. In healthy controls, BFI signals demonstrated minimal LFO power, reflecting a stable baseline hemodynamic state. However, in TBI patients, especially the comatose cases, elevated oscillatory activity was evident. These findings may reflect compensatory or dysregulated cerebrovascular responses following brain trauma. In particular, the increase in LFO power observed in deeper cortical regions (the late-gate data) suggests that the injured brain exhibits altered vascular dynamics. Increased oscillatory power has been linked to impaired autoregulation and vasomotor dysregulation in prior optical studies [38,41,43,45,50,51,53,133]. The MCS case showed higher baseline flow but less spectral power than coma, suggesting that partially preserved cortical function is associated with elevated CBF but less disorganized oscillatory activity, which is a well-documented consequence of TBI. A key strength of this study lies in the use of TD-DCS to extract depth-sensitive hemodynamic data. The EG primarily captured signals from superficial tissues, including the scalp and skull, while the LG isolated photons that traveled deeper into cerebral tissue. Our results confirm that both mean BFI and LFO power were higher in the LG than in the EG, especially in injured brains. This separation enabled us to discern whether observed changes stemmed from cortical processes or were confounded by extracerebral artifacts. This distinction is clinically relevant. Conventional CW-DCS systems are limited in this ability to resolve cortical signals, often leading to ambiguous interpretations of changes in flow. TD-DCS, particularly at longer wavelengths like 1064 nm,

498 overcomes this limitation by extending penetration depth and increasing specificity to cerebral
499 tissue. The late gate enhancement of oscillatory activity observed in TBI patients further supports
500 the cortical origin of these dynamics and validates the utility of depth gating for neurocritical care.

501 In addition to resting-state analysis, we evaluated functional reactivity using a smile protocol.
502 Healthy subjects exhibited clear task-evoked increases in both gates, corresponding to facial
503 motion (EG) and cortical activation (LG). The early gate signal showed a rapid rise within ~5
504 seconds of the verbal cue, consistent with superficial vasodilation and intact neurovascular
505 coupling, where superficial responses preceded slower, deeper hemodynamic activation. The late
506 gate response followed a canonical hemodynamic trajectory, characterized by a gradual rise, a
507 peak several seconds after stimulus onset, and a slow return to baseline, consistent with cortical
508 engagement. In contrast, the MCS patient exhibited smaller but temporally aligned responses in
509 both gates, suggesting partially preserved cortical reactivity despite limited behavioral output. The
510 comatose patient, who did not follow the verbal command, showed minimal modulation in the
511 early gate and a more rapid post-stimulus decline in the late gate signal. This pattern may indicate
512 severely diminished neurovascular coupling, impaired cortical engagement, and a loss of
513 sustained hemodynamic response. Notably, this BFI response profile parallels findings in task-
514 based fMRI, where the canonical BOLD signal typically peaks ~4-6 seconds after stimulus onset
515 in healthy individuals, reflecting increases in cerebral blood flow and volume in activated cortical
516 regions [77]. In patients with disorders of consciousness, attenuated BOLD responses have been
517 widely reported in response to auditory or motor commands, supporting the idea that impaired
518 neurovascular coupling contributes to reduced functional activation [71,73,74,134,135]. Similarly, EEG
519 studies in minimally conscious or vegetative patients often show reduced event-related potential
520 or cortical connectivity during tasks [30,136] . The attenuated LG response observed in our TD-DCS
521 measurements aligns with these prior findings, further validating TD-DCS as a functional imaging
522 tool capable of detecting residual cortical responsiveness. Together, these results highlight the
523 potential of TD-DCS to provide real-time, depth-resolved assessment of functional brain
524 responses and neurovascular integrity in critically ill patients at the bedside. The ability to non-
525 invasively measure cerebral LFOs and functional BFI responses at the bedside has significant
526 clinical implications. Current neuro-monitoring tools in the ICU are either invasive (e.g.,
527 intracranial pressure monitors), lack depth sensitivity (e.g., NIRS), or are not practical for
528 continuous use (e.g., MRI, PET). TD-DCS bridges this gap by offering portable, real-time
529 monitoring of both baseline perfusion and functional brain activity. In neurocritical care, LFO
530 patterns may serve as indicators of cerebrovascular health, injury severity, and recovery potential
531 [42,45,51]. Longitudinal tracking of LFOs and functional responses could help clinicians identify
532 patients at risk of secondary injury, evaluate the effectiveness of therapeutic interventions, and
533 guide decisions around sedation, rehabilitation, and prognosis.

534 While our findings are promising, several limitations warrant consideration. The patient data are
535 limited to five TBI cases, which restricts generalizability. Larger cohorts are needed to validate
536 LFO spectral changes as reliable markers of injury severity and recovery. Although time-gating
537 improves cerebral sensitivity, residual contamination from superficial tissues cannot be fully ruled
538 out. The β values derived from our $g_2$ fits were lower than standard CW-DCS systems due to the
539 use of few-mode fibers, although it enabled sufficient photon throughput for feasibility of human
540 brain measurements. Prior optical studies used ABP as an input function to assess autoregulation

through transfer-function analysis [121,123,133,137–141]. In this feasibility study, ABP was not recorded, so our interpretation relied on the output signal of TD-DCS. By normalizing PSD to total power, we focused on the relative distribution of oscillatory activity across bands. While this approach does not capture input-output coupling, it provides complementary information on depth-dependent cerebrovascular dynamics. Future work will incorporate systemic inputs for a more complete assessment of autoregulation. Combining TD-DCS with other modalities such as EEG or fNIRS may enhance spatial resolution and signal interpretation [38,124,125,142–144]. Future hardware development could explore optimized geometries that maintain high count rates while covering more spatial coverage. Longitudinal studies will be important to test whether TD-DCS metrics track recovery or deterioration over time.

## Conclusions

This study demonstrates the utility of TD-DCS as a noninvasive, depth-sensitive approach for monitoring cerebral blood flow (CBF) and low-frequency oscillations (LFOs) in the human brain. Our findings show that resting-state LFO power progressively decreases from healthy individuals to comatose patients, particularly in cortical regions, consistent with impaired neurovascular coupling and diminished autoregulatory function. Depth-sensitive analysis further reveals that these alterations are more pronounced in deeper layers, underscoring the value of late-gated measurements. Additionally, task-evoked changes in blood flow index (BFI) reveal preserved but attenuated hemodynamic responses in MCS and comatose patients, suggesting residual cortical reactivity despite impaired behavioral output. Together, these results highlight the promise of TD-DCS as a bedside tool for functional and physiological assessment in neurocritical care. With continued refinement and clinical validation, TD-DCS may serve as a valuable complement to existing neuroimaging modalities for real-time brain monitoring and prognostication in traumatic brain injury.

**Funding**

NIH R01 (NIBIB Brain Initiative, 7R01EB031759-03).

**Disclosures**

The authors declare the following potential conflicts of interest with respect to the research, authorship, and/or publication of this article: U.S and S.S. have a pending patent application relevant to this work.

**Code and Data Availability**

Data may be provided by the corresponding author upon reasonable request.

**Acknowledgements**

The authors acknowledge the funding support from NIH R01 (NIBIB Brain Initiative (7R01EB031759-03). We thank Nick Bertone (Picoquant Inc.) for providing the demo unit of HydraHarp400 for the time domain acquisition system. A pre-print version of this manuscript can be found on medRxiv, https://doi.org/10.1101/2025.08.31.25334647. ChatGPT (GPT-4) was used to assist with grammar and language editing during the preparation of this manuscript.

607

608 **References:**

609


610 1. S. L. James et al., “Global, regional, and national burden of traumatic brain injury and
611 spinal cord injury, 1990-2016: A systematic analysis for the Global Burden of Disease
612 Study 2016,” Lancet Neurol **18**(1), 56–87, Lancet Publishing Group (2019)
613 [doi:10.1016/S1474-4422(18)30415-0].

614 2. A. L. C. Zaninotto et al., “Traumatic brain injury,” in Clinical Trials in Neurology, F. Fregni,
615 Ed., Humana Press.

616 3. K. Kenney et al., “Cerebral Vascular Injury in Traumatic Brain Injury,” Exp Neurol **275**,
617 353–366, Academic Press Inc. (2016) [doi:10.1016/j.expneurol.2015.05.019].

618 4. B. Foreman et al., “Safety and Reliability of Bedside, Single Burr Hole Technique for
619 Intracranial Multimodality Monitoring in Severe Traumatic Brain Injury,” Neurocrit Care
620 **29**(3), 469–480, Neurocrit Care (2018) [doi:10.1007/S12028-018-0551-7].

621 5. D. K. Sandsmark et al., “Cerebral Microvascular Injury: A Potentially Treatable
622 Endophenotype of Traumatic Brain Injury-Induced Neurodegeneration,” in Neuron **103**(3),
623 pp. 367–379, Cell Press (2019) [doi:10.1016/j.neuron.2019.06.002].

624 6. C. Lazaridis and B. Foreman, “Management Strategies Based on Multi-Modality
625 Neuromonitoring in Severe Traumatic Brain Injury,” Neurotherapeutics **20**(6), 1457–1471,
626 Springer Science and Business Media Deutschland GmbH (2023) [doi:10.1007/S13311-
627 023-01411-2,].

628 7. P. Le Roux et al., “Consensus Summary Statement of the International Multidisciplinary
629 Consensus Conference on Multimodality Monitoring in Neurocritical Care: A statement for
630 healthcare professionals from the Neurocritical Care Society and the European Society of
631 Intensive Care Medicine,” Neurocrit Care **21**(2), 1–26, Humana Press Inc. (2014)
632 [doi:10.1007/s12028-014-0041-5].

633 8. H. Zhao et al., “Comparison of diffuse correlation spectroscopy analytical models for
634 measuring cerebral blood flow in adults,” J Biomed Opt **28**(12), SPIE-Intl Soc Optical Eng
635 (2023) [doi:10.1117/1.jbo.28.12.126005].

636 9. J. Selb et al., “Sensitivity of near-infrared spectroscopy and diffuse correlation
637 spectroscopy to brain hemodynamics: simulations and experimental findings during
638 hypercapnia,” Neurophotonics **1**(1), 15005, SPIE-Intl Soc Optical Eng (2014)
639 [doi:10.1117/1.nph.1.1.015005].

640 10. L. Qiu et al., “Time Domain Diffuse Correlation Spectroscopy for Detecting Human Brain
641 Function: Optimize System on Real Experimental Conditions by Simulation Method,”
642 IEEE Photonics J **13**(4), Institute of Electrical and Electronics Engineers Inc. (2021)
643 [doi:10.1109/JPHOT.2021.3089635].

644 11. J. Selb et al., “Prolonged monitoring of cerebral blood flow and autoregulation with diffuse
645 correlation spectroscopy in neurocritical care patients,” Neurophotonics **5**(04), 1, SPIE-
646 Intl Soc Optical Eng (2018) [doi:10.1117/1.NPH.5.4.045005,].

12. D. Mazumder et al., “Optimization of time domain diffuse correlation spectroscopy parameters for measuring brain blood flow,” Neurophotonics **8**(03), SPIE-Intl Soc Optical Eng (2021) [doi:10.1117/1.NPH.8.3.035005,].

13. D. A. Boas et al., “Establishing the diffuse correlation spectroscopy signal relationship with blood flow,” Neurophotonics **3**(3), 31412, SPIE-Intl Soc Optical Eng (2016) [doi:10.1117/1.NPH.3.3.031412,].

14. F. Amyot et al., “A Review of the Effectiveness of Neuroimaging Modalities for the Detection of Traumatic Brain Injury,” J Neurotrauma **32**(22), 1693–1721, Mary Ann Liebert Inc. (2015) [doi:10.1089/NEU.2013.3306,].

15. X. Cheng et al., “Measuring neuronal activity with diffuse correlation spectroscopy: a theoretical investigation,” Neurophotonics **8**(03), SPIE-Intl Soc Optical Eng (2021) [doi:10.1117/1.NPH.8.3.035004,].

16. J. Li et al., “Characterization of autism spectrum disorder with spontaneous hemodynamic activity,” Biomed Opt Express **7**(10), 3871, Optica Publishing Group (2016) [doi:10.1364/BOE.7.003871,].

17. J. Sutin et al., “Time-domain diffuse correlation spectroscopy,” Optica **3**(9), 1006, Optica Publishing Group (2016) [doi:10.1364/OPTICA.3.001006,].

18. O. Kholiqov et al., “Time-of-flight resolved light field fluctuations reveal deep human tissue physiology,” Nature Communications 2020 11:1 **11**(1), 391-, Nature Publishing Group (2020) [doi:10.1038/s41467-019-14228-5].

19. W. Zhou et al., “Multi-exposure interferometric diffusing wave spectroscopy,” Optics Letters, Vol. 46, Issue 18, pp. 4498-4501 **46**(18), 4498–4501, Optica Publishing Group (2021) [doi:10.1364/OL.427746].

20. L. Qiu et al., “Analytical models for time-domain diffuse correlation spectroscopy for multi-layer and heterogeneous turbid media,” Biomedical Optics Express, Vol. 8, Issue 12, pp. 5518-5532 **8**(12), 5518–5532, Optica Publishing Group (2017) [doi:10.1364/BOE.8.005518].

21. L. Qiu et al., “Using a simulation approach to optimize time-domain diffuse correlation spectroscopy measurement on human head,” Neurophotonics **5**(2), 1, Neurophotonics (2018) [doi:10.1117/1.NPH.5.2.025007].

22. T. Ko et al., “Fast blood flow monitoring in deep tissues with real-time software correlators,” Biomedical Optics Express, Vol. 7, Issue 3, pp. 776-797 **7**(3), 776–797, Optica Publishing Group (2016) [doi:10.1364/BOE.7.000776].

23. C.-S. Poon et al., “First-in-clinical application of a time-gated diffuse correlation spectroscopy system at 1064 nm using superconducting nanowire single photon detectors in a neuro intensive care unit,” Biomed Opt Express **13**(3), 1344, Optica Publishing Group (2022) [doi:10.1364/boe.448135].

24. M. Pagliazzi et al., “In vivo time domain speckle contrast optical spectroscopy,” in European Conference on Biomedical Optics, Optica Publishing Group.

686 25. C. S. Poon et al., “Noninvasive optical monitoring of cerebral blood flow and eeg spectral
687 responses after severe traumatic brain injury: A case report,” Brain Sci **11**(8), MDPI
688 (2021) [doi:10.3390/brainsci11081093].

689 26. V. Parfentyeva et al., “Fast time-domain diffuse correlation spectroscopy with
690 superconducting nanowire single-photon detector: system validation and in vivo results,”
691 Sci Rep **13**(1), Nature Research (2023) [doi:10.1038/s41598-023-39281-5].

692 27. N. Ozana et al., “Superconducting nanowire single-photon sensing of cerebral blood
693 flow,” Neurophotonics **8**(3), Neurophotonics (2021) [doi:10.1117/1.NPH.8.3.035006].

694 28. J. Li et al., “Resting-state functional connectivity measured by diffuse correlation
695 spectroscopy,” J Biophotonics **11**(2), J Biophotonics (2018)
696 [doi:10.1002/JBIO.201700165].

697 29. D. R. Busch et al., “Continuous cerebral hemodynamic measurement during deep
698 hypothermic circulatory arrest,” Biomed Opt Express **7**(9), 3461, Optica Publishing Group
699 (2016) [doi:10.1364/BOE.7.003461,].

700 30. E. S. Rosenthal et al., “Continuous Electroencephalography Predicts Delayed Cerebral
701 Ischemia after Subarachnoid Hemorrhage: A Prospective Study of Diagnostic Accuracy,”
702 Ann Neurol **83**(5), 958, John Wiley and Sons Inc. (2018) [doi:10.1002/ANA.25232].

703 31. M. Mohtasebi et al., “Detection of low-frequency oscillations in neonatal piglets with
704 speckle contrast diffuse correlation tomography,” J Biomed Opt **28**(12), 121204, SPIE-Intl
705 Soc Optical Eng (2023) [doi:10.1117/1.JBO.28.12.121204].

706 32. W. B. Baker et al., “Continuous non-invasive optical monitoring of cerebral blood flow and
707 oxidative metabolism after acute brain injury,” Journal of Cerebral Blood Flow and
708 Metabolism **39**(8), 1469–1485, SAGE Publications Ltd (2019)
709 [doi:10.1177/0271678X19846657,].

710 33. D. J. Davies et al., “Cerebral oxygenation in traumatic brain injury: Can a non-invasive
711 frequency domain near-infrared spectroscopy device detect changes in brain tissue
712 oxygen tension as well as the established invasive monitor?,” J Neurotrauma **36**(7),
713 1175–1183, Mary Ann Liebert Inc. (2019) [doi:10.1089/NEU.2018.5667,].

714 34. C. Du et al., “Low-frequency calcium oscillations accompany deoxyhemoglobin
715 oscillations in rat somatosensory cortex,” Proc Natl Acad Sci U S A **111**(43), E4677–
716 E4686, National Academy of Sciences (2014) [doi:10.1073/pnas.1410800111].

717 35. W. Chen et al., “Cocaine Decreases Spontaneous Neuronal Activity and Increases Low-
718 Frequency Neuronal and Hemodynamic Cortical Oscillations,” Cerebral Cortex **29**(4),
719 1594–1606, Oxford University Press (2019) [doi:10.1093/cercor/bhy057].

720 36. R. Cheng et al., “Noninvasive optical evaluation of spontaneous low frequency
721 oscillations in cerebral hemodynamics,” Neuroimage **62**(3), 1445–1454 (2012)
722 [doi:10.1016/j.neuroimage.2012.05.069].

723 37. Y. Li et al., “Systemic low-frequency oscillations observed in the periphery of healthy
724 human subjects,” J Biomed Opt **23**(05), 1, SPIE-Intl Soc Optical Eng (2018)
725 [doi:10.1117/1.JBO.23.5.057001,].

38. G. Bicciato et al., “Increase in Low-Frequency Oscillations in fNIRS as Cerebral Response to Auditory Stimulation with Familiar Music,” Brain Sci **12**(1), 42, MDPI (2021) [doi:10.3390/BRAINSCI12010042].

39. C. Yaramothu et al., “Reliability of Frontal Eye Fields Activation and Very Low-Frequency Oscillations Observed during Vergence Eye Movements: an fNIRS Study,” Sci Rep **10**(1), 1–10, Nature Research (2020) [doi:10.1038/S41598-020-57597-4;TECHMETA=5,59;SUBJMETA=2613,378,3920,631;KWRD=NEURAL+CIRCUITS,VISUAL+SYSTEM].

40. C. Yaramothu et al., “Reliability of Frontal Eye Fields Activation and Very Low-Frequency Oscillations Observed during Vergence Eye Movements: an fNIRS Study,” Scientific Reports 2020 10:1 **10**(1), 712-, Nature Publishing Group (2020) [doi:10.1038/s41598-020-57597-4].

41. A. V. Andersen et al., “Assessing low-frequency oscillations in cerebrovascular diseases and related conditions with near-infrared spectroscopy: a plausible method for evaluating cerebral autoregulation?,” Neurophotonics **5**(3), 30901, SPIE-Intl Soc Optical Eng (2018) [doi:10.1117/1.NPH.5.3.030901].

42. Y. Tong et al., “Low-frequency oscillations measured in the periphery with near-infrared spectroscopy are strongly correlated with blood oxygen level-dependent functional magnetic resonance imaging signals,” J Biomed Opt **17**(10), 1, SPIE-Intl Soc Optical Eng (2012) [doi:10.1117/1.JBO.17.10.106004,].

43. V. Chernomordik et al., “Abnormality of low frequency cerebral hemodynamics oscillations in TBI population,” Brain Res **1639**, 194–199, Elsevier B.V. (2016) [doi:10.1016/j.brainres.2016.02.018].

44. M. Y. Wang et al., “Functional near-infrared spectroscopy can detect low-frequency hemodynamic oscillations in the prefrontal cortex during steady-state visual evoked potential-inducing periodic facial expression stimuli presentation,” Vis Comput Ind Biomed Art **3**(1), 1–8, Springer Science and Business Media B.V. (2020) [doi:10.1186/S42492-020-00065-7/FIGURES/8].

45. S. Schulthess et al., “Low frequency oscillations reflect neurovascular coupling and disappear after cerebral death,” Scientific Reports 2024 14:1 **14**(1), 1–10, Nature Publishing Group (2024) [doi:10.1038/s41598-024-61819-4].

46. D. Phillip et al., “Low frequency oscillations in cephalic vessels assessed by near infrared spectroscopy,” Eur J Clin Invest **42**(11), 1180–1188, Eur J Clin Invest (2012) [doi:10.1111/J.1365-2362.2012.02704.X,].

47. H. Obrig et al., “Spontaneous low frequency oscillations of cerebral hemodynamics and metabolism in human adults,” Neuroimage **12**(6), 623–639, Academic Press Inc. (2000) [doi:10.1006/nimg.2000.0657].

48. C. Yeo et al., “Low frequency oscillations assessed by diffuse speckle contrast analysis for foot angiosome concept,” Scientific Reports 2020 10:1 **10**(1), 1–14, Nature Publishing Group (2020) [doi:10.1038/s41598-020-73604-0].

49. Y. Tong, L. M. Hocke, and B. B. Frederick, “Low Frequency Systemic Hemodynamic ‘Noise’ in Resting State BOLD fMRI: Characteristics, Causes, Implications, Mitigation Strategies, and Applications,” Front Neurosci **13**(JUL), 787, Frontiers Media S.A. (2019) [doi:10.3389/FNINS.2019.00787].

50. A. Vermeij et al., “Very-low-frequency oscillations of cerebral hemodynamics and blood pressure are affected by aging and cognitive load,” Neuroimage **85**, 608–615, Neuroimage (2014) [doi:10.1016/j.neuroimage.2013.04.107].

51. B. R. White et al., “Low frequency power in cerebral blood flow is a biomarker of neurologic injury in the acute period after cardiac arrest,” Resuscitation **178**, 12–18, Elsevier Ireland Ltd (2022) [doi:10.1016/j.resuscitation.2022.07.004].

52. M. J. Lowe, B. J. Mock, and J. A. Sorenson, “Functional Connectivity in Single and Multislice Echoplanar Imaging Using Resting-State Fluctuations,” Neuroimage **7**(2), 119–132, Academic Press (1998) [doi:10.1006/NIMG.1997.0315].

53. N. Lodha and E. A. Christou, “Low-Frequency Oscillations and Control of the Motor Output,” Front Physiol **8**(FEB), 78, Frontiers Research Foundation (2017) [doi:10.3389/FPHYS.2017.00078].

54. J. Selb et al., “Prolonged monitoring of cerebral blood flow and autoregulation with diffuse correlation spectroscopy in neurocritical care patients,” Neurophotonics **5**(04), 1, SPIE-Intl Soc Optical Eng (2018) [doi:10.1117/1.NPH.5.4.045005,].

55. W. B. Baker et al., “Continuous non-invasive optical monitoring of cerebral blood flow and oxidative metabolism after acute brain injury,” Journal of Cerebral Blood Flow and Metabolism **39**(8), 1469–1485, SAGE Publications Ltd (2019) [doi:10.1177/0271678X19846657,].

56. D. R. Busch et al., “Detection of Brain Hypoxia Based on Noninvasive Optical Monitoring of Cerebral Blood Flow with Diffuse Correlation Spectroscopy,” Neurocrit Care **30**(1), 72–80, Humana Press Inc. (2019) [doi:10.1007/S12028-018-0573-1,].

57. R. M. Forti et al., “Transcranial Optical Monitoring of Cerebral Hemodynamics in Acute Stroke Patients during Mechanical Thrombectomy,” Journal of Stroke and Cerebrovascular Diseases **28**(6), 1483–1494, W.B. Saunders (2019) [doi:10.1016/J.JSTROKECEREBROVASDIS.2019.03.019].

58. T. Durduran and A. G. Yodh, “Diffuse correlation spectroscopy for non-invasive, micro-vascular cerebral blood flow measurement,” Neuroimage **85**(0 1), 51, Academic Press Inc. (2014) [doi:10.1016/j.neuroimage.2013.06.017].

59. M. N. Kim et al., “Continuous optical monitoring of cerebral hemodynamics during head-of-bed manipulation in brain-injured adults,” Neurocrit Care **20**(3), 443–453, Humana Press Inc. (2014) [doi:10.1007/S12028-013-9849-7/FIGURES/2].

60. C. G. Favilla et al., “Optical bedside monitoring of cerebral blood flow in acute ischemic stroke patients during head-of-bed manipulation,” Stroke **45**(5), 1269–1274, Lippincott Williams and Wilkins (2014) [doi:10.1161/STROKEAHA.113.004116/-/DC1].

61. E. M. Buckley et al., “Diffuse correlation spectroscopy for measurement of cerebral blood flow: future prospects,” Neurophotonics **1**(1), 11009, SPIE-Intl Soc Optical Eng (2014) [doi:10.1117/1.NPh.1.1.011009].

62. H. L et al., “Noninvasive continuous optical monitoring of absolute cerebral blood flow in critically ill adults,” Neurophotonics **5**(4), 1, Neurophotonics (2018) [doi:10.1117/1.NPH.5.4.045006].

63. M. Diop et al., “Development of a combined broadband near-infrared and diffusion correlation system for monitoring cerebral blood flow and oxidative metabolism in preterm infants,” Biomed Opt Express **6**(10) (2015) [doi:10.1364/boe.6.003907].

64. K. Verdecchia et al., “Quantifying the cerebral metabolic rate of oxygen by combining diffuse correlation spectroscopy and time-resolved near-infrared spectroscopy,” J Biomed Opt (2013) [doi:10.1117/1.jbo.18.2.027007].

65. M. Suwalski et al., “The Effect of Hypotension on Cerebral Metabolism and Perfusion in Adults Undergoing Cardiopulmonary Bypass: A Prospective Cohort Study,” Anesth Analg **141**(5), Anesth Analg (2025) [doi:10.1213/ANE.0000000000007607].

66. A. Demertzi et al., “Intrinsic functional connectivity differentiates minimally conscious from unresponsive patients,” Brain **138**(Pt 9), 2619–2631, Brain (2015) [doi:10.1093/BRAIN/AWV169].

67. J. T. Giacino et al., “The minimally conscious state: Definition and diagnostic criteria,” Neurology **58**(3) (2002) [doi:10.1212/WNL.58.3.349].

68. H. Lu et al., “A functional near-infrared spectroscopy study on hemodynamic changes of patients with prolonged disorders of consciousness responding to different auditory stimuli,” BMC Neurology 2023 23:1 **23**(1), 242-, BioMed Central (2023) [doi:10.1186/S12883-023-03292-6].

69. M. Li et al., “Detecting Residual Awareness in Patients With Prolonged Disorders of Consciousness: An fNIRS Study,” Front Neurol **12**, Front Neurol (2021) [doi:10.3389/FNEUR.2021.618055].

70. G. Bicciato et al., “Functional NIRS to detect covert consciousness in neurocritical patients,” Clinical Neurophysiology **144**, 72–82, Elsevier Ireland Ltd (2022) [doi:10.1016/j.clinph.2022.10.002].

71. M. M. Monti et al., “Willful modulation of brain activity in disorders of consciousness,” N Engl J Med **362**(7), 579–589, N Engl J Med (2010) [doi:10.1056/NEJMOA0905370].

72. A. M. Owen et al., “Detecting awareness in the vegetative state,” Science **313**(5792), 1402, Science (2006) [doi:10.1126/SCIENCE.1130197].

73. M. Boly et al., “Functional connectivity in the default network during resting state is preserved in a vegetative but not in a brain dead patient,” Hum Brain Mapp **30**(8), 2393 (2009) [doi:10.1002/HBM.20672].

74. J. Stender et al., “Diagnostic precision of PET imaging and functional MRI in disorders of consciousness: A clinical validation study,” The Lancet **384**(9942), 514–522, Elsevier B.V. (2014) [doi:10.1016/S0140-6736(14)60042-8].

75. B. Hermann et al., “Multimodal FDG-PET and EEG assessment improves diagnosis and prognostication of disorders of consciousness,” Neuroimage Clin **30**, 102601, Elsevier (2021) [doi:10.1016/J.NICL.2021.102601].

76. J. T. Giacino et al., “Comprehensive systematic review update summary: Disorders of consciousness: Report of the Guideline Development, Dissemination, and Implementation Subcommittee of the American Academy of Neurology; the American Congress of Rehabilitation Medicine; and th…,” Neurology **91**(10), 461, Lippincott Williams and Wilkins (2018) [doi:10.1212/WNL.0000000000005928].

77. F. Dondi et al., “The Role of [18F]FDG PET Imaging for the Assessment of Vegetative State or Unresponsive Wakefulness Syndrome: A Systematic Review,” Diagnostics **15**(11), 1406, Multidisciplinary Digital Publishing Institute (MDPI) (2025) [doi:10.3390/DIAGNOSTICS15111406/S1].

78. C. C. H. Lo, P. Y. M. Woo, and V. C. K. Cheung, “Task-based EEG and fMRI paradigms in a multimodal clinical diagnostic framework for disorders of consciousness,” Rev Neurosci **35**(7), 775–787, Rev Neurosci (2024) [doi:10.1515/REVNEURO-2023-0159].

79. H. Huang et al., “Early Consciousness Disorder in Acute Large Hemispheric Infarction: An Analysis Based on Quantitative EEG and Brain Network Characteristics,” Neurocrit Care **33**(2), 376–388, Springer (2020) [doi:10.1007/s12028-020-01051-w].

80. J. Claassen et al., “Detection of Brain Activation in Unresponsive Patients with Acute Brain Injury,” N Engl J Med **380**(26), 2497–2505, N Engl J Med (2019) [doi:10.1056/NEJMOA1812757].

81. J. Claassen et al., “Detection of Brain Activation in Unresponsive Patients with Acute Brain Injury,” New England Journal of Medicine **380**(26), 2497–2505, Massachusetts Medical Society (2019) [doi:10.1056/NEJMOA1812757;WGROUP:STRING:MMS].

82. P. Le Roux et al., “Consensus Summary Statement of the International Multidisciplinary Consensus Conference on Multimodality Monitoring in Neurocritical Care: A statement for healthcare professionals from the Neurocritical Care Society and the European Society of Intensive Care Medicine,” Neurocrit Care **21**(2), 1–26, Humana Press Inc. (2014) [doi:10.1007/s12028-014-0041-5].

83. K. Kazazian et al., “Functional near-infrared spectroscopy: A novel tool for detecting consciousness after acute severe brain injury,” Proceedings of the National Academy of Sciences **121**(36), e2402723121, National Academy of Sciences (2024) [doi:10.1073/PNAS.2402723121].

84. M. H. Othman et al., “Resting-State NIRS–EEG in Unresponsive Patients with Acute Brain Injury: A Proof-of-Concept Study,” Neurocrit Care **34**(1) (2021) [doi:10.1007/s12028-020-00971-x].

881 85. G. Bicciato et al., “Functional NIRS to detect covert consciousness in neurocritical
882 patients,” Clinical Neurophysiology **144**, 72–82 (2022)
883 [doi:https://doi.org/10.1016/j.clinph.2022.10.002].

884 86. L. Bastian et al., “Sensitive and specific fNIRS-based approach for awareness detection
885 in disorders of consciousness: proof of principle in healthy adults,” Neurophotonics **12**(4),
886 Neurophotonics (2025) [doi:10.1117/1.NPH.12.4.045001].

887 87. Y. Bai, Y. Lin, and U. Ziemann, “Managing disorders of consciousness: the role of
888 electroencephalography,” J Neurol **268**(11), 4033, Springer Science and Business Media
889 Deutschland GmbH (2020) [doi:10.1007/S00415-020-10095-Z].

890 88. J. D. Sitt et al., “Large scale screening of neural signatures of consciousness in patients
891 in a vegetative or minimally conscious state,” Brain **137**(8), 2258–2270, Oxford Academic
892 (2014) [doi:10.1093/BRAIN/AWU141].

893 89. E. Kirilina et al., “The physiological origin of task-evoked systemic artefacts in functional
894 near infrared spectroscopy,” Neuroimage **61**(1), 70–81, Academic Press (2012)
895 [doi:10.1016/J.NEUROIMAGE.2012.02.074].

896 90. U. Chaudhary et al., “Brain–Computer Interface–Based Communication in the Completely
897 Locked-In State,” PLoS Biol **15**(1), e1002593, Public Library of Science (2017)
898 [doi:10.1371/JOURNAL.PBIO.1002593].

899 91. Y. Wang et al., “Detecting cognitive motor dissociation by functional near-infrared
900 spectroscopy,” Front Neurol **16**, 1532804, Frontiers Media SA (2025)
901 [doi:10.3389/FNEUR.2025.1532804/FULL].

902 92. G. B. Narula et al., “Functional NIRS to detect covert consciousness in neurocritical
903 patients,” Clin. Neurophysiol **144**, 72–82.

904 93. M. M. Monti et al., “Willful Modulation of Brain Activity in Disorders of Consciousness,”
905 New England Journal of Medicine **362**(7), 579–589, Massachusetts Medical Society
906 (2010) [doi:10.1056/NEJMOA0905370;WGROUP:STRING:MMS].

907 94. C. C. H. Lo, P. Y. M. Woo, and V. C. K. Cheung, “Task-based EEG and fMRI paradigms
908 in a multimodal clinical diagnostic framework for disorders of consciousness,” Rev
909 Neurosci **35**(7), 775–787, Rev Neurosci (2024) [doi:10.1515/REVNEURO-2023-0159].

910 95. E. M. Buckley et al., “Diffuse correlation spectroscopy for measurement of cerebral blood
911 flow: future prospects,” https://doi.org/10.1117/1.NPh.1.1.011009 **1**(1), 11009, SPIE
912 (2014) [doi:10.1117/1.NPH.1.1.011009].

913 96. L. Cortese et al., “Recipes for diffuse correlation spectroscopy instrument design using
914 commonly utilized hardware based on targets for signal-to-noise ratio and precision,”
915 Biomedical Optics Express, Vol. 12, Issue 6, pp. 3265-3281 **12**(6), 3265–3281, Optica
916 Publishing Group (2021) [doi:10.1364/BOE.423071].

917 97. D. R. Busch et al., “Laser safety in fiber-optic monitoring of spinal cord hemodynamics: a
918 preclinical evaluation,” J Biomed Opt (2018) [doi:10.1117/1.jbo.23.6.065003].

98. L. Qiu et al., “Using a simulation approach to optimize time-domain diffuse correlation spectroscopy measurement on human head,” Neurophotonics **5**(02), 1 (2018) [doi:10.1117/1.nph.5.2.025007].

99. J. Li et al., “Analytical models for time-domain diffuse correlation spectroscopy for multi-layer and heterogeneous turbid media,” Biomed Opt Express **8**(12), 5518, Optica Publishing Group (2017) [doi:10.1364/BOE.8.005518,].

100. S. A. Carp et al., “Diffuse correlation spectroscopy measurements of blood flow using 1064 nm light,” J Biomed Opt **25**(9), J Biomed Opt (2020) [doi:10.1117/1.JBO.25.9.097003].

101. L. Colombo et al., “In vivo time-domain diffuse correlation spectroscopy above the water absorption peak,” Opt Lett **45**(13), 3377, Optica Publishing Group (2020) [doi:10.1364/ol.392355].

102. T. Durduran and A. G. Yodh, “Diffuse correlation spectroscopy for non-invasive, micro-vascular cerebral blood flow measurement,” Neuroimage **85**(0 1), 51, Academic Press Inc. (2014) [doi:10.1016/j.neuroimage.2013.06.017].

103. D. A. Boas and A. G. Yodh, “Spatially varying dynamical properties of turbid media probed with diffusing temporal light correlation,” Journal of The Optical Society of America A-optics Image Science and Vision **14**(1), 192, Optica Publishing Group (1997) [doi:10.1364/JOSAA.14.000192].

104. D. A. Boas, L. E. Campbell, and A. G. Yodh, “Scattering and imaging with diffusing temporal field correlations,” Phys Rev Lett **75**(9), 1855–1858, Phys Rev Lett (1995) [doi:10.1103/PHYSREVLETT.75.1855,].

105. R. C. Mesquita et al., “Direct measurement of tissue blood flow and metabolism with diffuse optics,” Philosophical Transactions of the Royal Society A: Mathematical, Physical and Engineering Sciences **369**(1955), 4390–4406, The Royal Society Publishing (2011) [doi:10.1098/RSTA.2011.0232].

106. M. N. Kim et al., “Continuous optical monitoring of cerebral hemodynamics during head-of-bed manipulation in brain-injured adults,” Neurocrit Care **20**(3), 443–453, Humana Press Inc. (2014) [doi:10.1007/S12028-013-9849-7/FIGURES/2].

107. D. Tamborini et al., “Portable System for Time-Domain Diffuse Correlation Spectroscopy,” IEEE Trans Biomed Eng **66**(11), 3014–3025, IEEE Computer Society (2019) [doi:10.1109/TBME.2019.2899762].

108. R. Erdmann et al., “Time domain diffuse correlation spectroscopy with a high coherence pulsed source: in vivo and phantom results,” Biomedical Optics Express, Vol. 8, Issue 11, pp. 5311-5325 **8**(11), 5311–5325, Optica Publishing Group (2017) [doi:10.1364/BOE.8.005311].

109. L. Shi et al., “Transmission in near-infrared optical windows for deep brain imaging,” J Biophotonics **9**(1–2), 38–43, Wiley-VCH Verlag (2016) [doi:10.1002/JBIO.201500192;PAGEGROUP:STRING:PUBLICATION].

110. L. A. Sordillo et al., “Deep optical imaging of tissue using the second and third near-infrared spectral windows,” https://doi.org/10.1117/1.JBO.19.5.056004 **19**(5), 56004, SPIE (2014) [doi:10.1117/1.JBO.19.5.056004].

111. W. Liu et al., “Fast and sensitive diffuse correlation spectroscopy with highly parallelized single photon detection,” APL Photonics **6**(2), 26106, American Institute of Physics Inc. (2021) [doi:10.1063/5.0031225/1062592].

112. M. Azimipour et al., “Fluorescence laminar optical tomography for brain imaging: system implementation and performance evaluation,” J Biomed Opt **22**(1), 2017/01/06, 16003 (2017) [doi:10.1117/1.JBO.22.1.016003].

113. C. Poon et al., “Cerebral blood flow-based resting state functional connectivity of the human brain using optical diffuse correlation spectroscopy,” Journal of Visualized Experiments **2020**(159), 1–7, Journal of Visualized Experiments (2020) [doi:10.3791/60765,].

114. A. Pifferi et al., “Time-resolved diffuse reflectance using small source-detector separation and fast single-photon gating,” Phys Rev Lett **100**(13), Phys Rev Lett (2008) [doi:10.1103/PHYSREVLETT.100.138101,].

115. L. Colombo et al., “Effects of the instrument response function and the gate width in time-domain diffuse correlation spectroscopy: model and validations,” https://doi.org/10.1117/1.NPh.6.3.035001 **6**(3), 35001, SPIE (2019) [doi:10.1117/1.NPH.6.3.035001].

116. S. Samaei et al., “Time-domain diffuse correlation spectroscopy (TD-DCS) for noninvasive, depth-dependent blood flow quantification in human tissue in vivo,” Sci Rep **11**(1), Nature Research (2021) [doi:10.1038/s41598-021-81448-5].

117. S. Tagliabue et al., “How the heterogeneity of the severely injured brain affects hybrid diffuse optical signals: case examples and guidelines,” Neurophotonics **11**(4), Neurophotonics (2024) [doi:10.1117/1.NPH.11.4.045005].

118. W. Chen et al., “Interactions between stimuli-evoked cortical activity and spontaneous low frequency oscillations measured with neuronal calcium,” Neuroimage **210**, Academic Press Inc. (2020) [doi:10.1016/J.NEUROIMAGE.2020.116554,].

119. D. S. Langri and U. Sunar, “Non-Invasive Continuous Optical Monitoring of Cerebral Blood Flow after Traumatic Brain Injury in Mice Using Fiber Camera-Based Speckle Contrast Optical Spectroscopy,” Brain Sci **13**(10), Multidisciplinary Digital Publishing Institute (MDPI) (2023) [doi:10.3390/BRAINSCI13101365,].

120. A. Fanta et al., “Assessment of cerebral autoregulation and cerebral perfusion in patients with sickle cell disease using frequency-domain near-infrared spectroscopy,” J Appl Physiol **139**(3), 638–649, American Physiological Society (2025) [doi:10.1152/JAPPLPHYSIOL.00426.2023].

121. N. F. Chi et al., “Dynamic Cerebral Autoregulation Is an Independent Functional Outcome Predictor of Mild Acute Ischemic Stroke,” Stroke **49**(11), 2605–2611, Stroke (2018) [doi:10.1161/STROKEAHA.118.022481].

122. H. Cheng et al., “Power spectrum of spontaneous cerebral homodynamic oscillation shows a distinct pattern in autism spectrum disorder,” Biomed Opt Express **10**(3), 1383, Biomed Opt Express (2019) [doi:10.1364/BOE.10.001383].

123. S. Wood et al., “Assessing Dynamic Cerebral Autoregulation in Patients with Sickle Cell Disease Using Near-Infrared Spectroscopy and Paced Breathing,” Blood **136**(Supplement 1), 57–58, American Society of Hematology (2020) [doi:10.1182/BLOOD-2020-137624].

124. Y. Tong and B. Frederick, “Concurrent fNIRS and fMRI processing allows independent visualization of the propagation of pressure waves and bulk blood flow in the cerebral vasculature,” Neuroimage **61**, 1419–1427.

125. L. Duan, Y. J. Zhang, and C. Z. Zhu, “Quantitative comparison of resting-state functional connectivity derived from fNIRS and fMRI: A simultaneous recording study,” Neuroimage **60**, 2008–2018.

126. S. Schulthess et al., “Low frequency oscillations reflect neurovascular coupling and disappear after cerebral death,” Scientific Reports 2024 14:1 **14**(1), 1–10, Nature Publishing Group (2024) [doi:10.1038/s41598-024-61819-4].

127. S. Chennu et al., “Brain networks predict metabolism, diagnosis and prognosis at the bedside in disorders of consciousness,” Brain **140**(8), 2120–2132, Brain (2017) [doi:10.1093/BRAIN/AWX163].

128. A. Soddu et al., “Resting state activity in patients with disorders of consciousness,” Funct Neurol **26**(1), 37 (2011).

129. S. Laureys, A. M. Owen, and N. D. Schiff, “Brain function in coma, vegetative state, and related disorders,” Lancet Neurology **3**(9), 537–546, Lancet Neurol (2004) [doi:10.1016/S1474-4422(04)00852-X].

130. O. Gosseries et al., “Disorders of consciousness: what’s in a name?,” NeuroRehabilitation **28**(1), 3–14, NeuroRehabilitation (2011) [doi:10.3233/NRE-2011-0625].

131. L. Colombo et al., “In vivo time-domain diffuse correlation spectroscopy above the water absorption peak,” Opt Lett **45**(13), 3377, Optica Publishing Group (2020) [doi:10.1364/ol.392355].

132. B. R. White et al., “Low frequency power in cerebral blood flow is a biomarker of neurologic injury in the acute period after cardiac arrest,” Resuscitation **178**, 12–18, Elsevier Ireland Ltd (2022) [doi:10.1016/j.resuscitation.2022.07.004].

133. A. Sassaroli et al., “Low-frequency spontaneous oscillations of cerebral hemodynamics investigated with near-infrared spectroscopy: A review,” in IEEE Journal on Selected Topics in Quantum Electronics **18**(4) (2012) [doi:10.1109/JSTQE.2012.2183581].

134. Y. Tong, L. M. Hocke, and B. B. Frederick, “Low Frequency Systemic Hemodynamic ‘Noise’ in Resting State BOLD fMRI: Characteristics, Causes, Implications, Mitigation Strategies, and Applications,” Front Neurosci **13**(JUL), 787, Frontiers Media S.A. (2019) [doi:10.3389/FNINS.2019.00787].

135. C. D. Schaper, “Analytic Model of fMRI BOLD Signals for Separable Metrics of Neural and Metabolic Activity,” bioRxiv, 573006 (2019) [doi:10.1101/573006].

136. B. Foreman et al., “Intracortical electrophysiological correlates of blood flow after severe SAH: A multimodality monitoring study,” Journal of Cerebral Blood Flow and Metabolism **38**(3), 506–517, SAGE Publications Ltd (2018) [doi:10.1177/0271678X17700433,].

137. J. M. Kainerstorfer et al., “Cerebral autoregulation in the microvasculature measured with near-infrared spectroscopy,” J Cereb Blood Flow Metab **35**(6), 959–966, J Cereb Blood Flow Metab (2015) [doi:10.1038/JCBFM.2015.5].

138. D. Phillip et al., “Spontaneous Low Frequency Oscillations in Acute Ischemic Stroke – A Near Infrared Spectroscopy (NIRS) Study” (2014) [doi:10.4172/2155-9562.1000241].

139. A. Fanta et al., “Assessment of cerebral autoregulation and cerebral perfusion in patients with sickle cell disease using frequency-domain near-infrared spectroscopy,” J Appl Physiol (1985) **139**(3), 638–649, J Appl Physiol (1985) (2025) [doi:10.1152/JAPPLPHYSIOL.00426.2023].

140. R. C. Nogueira et al., “Review of studies on dynamic cerebral autoregulation in the acute phase of stroke and the relationship with clinical outcome,” J Cereb Blood Flow Metab **42**(3), 430–453, J Cereb Blood Flow Metab (2022) [doi:10.1177/0271678X211045222].

141. H. Cheng et al., “Power spectrum of spontaneous cerebral homodynamic oscillation shows a distinct pattern in autism spectrum disorder,” Biomed. Opt. Express **10**, 1383–1392.

142. C. M. Lu et al., “Use of fNIRS to assess resting state functional connectivity,” J. Neurosci. Methods **186**, 242–249.

143. R. F. Rojas et al., “Physiological fluctuations show frequency-specific networks in fNIRS signals during resting state,” in Proceedings of the 39th Annual International Conference of the IEEE Engineering in Medicine and Biology Society, Jeju, Republic of Korea.

144. B. Foreman and J. Claassen, “Quantitative EEG for the detection of brain ischemia,” Crit Care **16**(2), Crit Care (2012) [doi:10.1186/CC11230,].